Effect of breaking cylindrical symmetry on photoelectron angular distributions resulting from resonance-enhanced two-photon ionization

Katharine L. Reid, David J. Leahy, and Richard N. Zare
Department of Chemistry, Stanford University, Stanford, California 94305

(Received 18 January 1991; accepted 29 March 1991)

An expression is derived for the photoelectron angular distribution (PAD) following $(1+1')$ resonance-enhanced multiphoton ionization (REMPI) of a molecule with linearly polarized light beams. When the two polarization vectors are parallel, cylindrical symmetry exists, and the PAD depends only on θ, the angle between the linear polarization vector of the ionizing radiation and the electron ejection direction. When the polarization vectors are perpendicular, cylindrical symmetry is broken, and the PAD shows ϕ and θ dependence. For an arbitrary angle between the two polarization vectors, the angular distribution ceases to have reflection symmetry. This breaking of cylindrical symmetry causes interference effects in the REMPI process that are readily described using a density matrix formalism. As an example, the $(1+1')$ REMPI of NO via its $A\,^2\Sigma^+$ state is considered.

I. INTRODUCTION

Photoelectron angular distributions (PADs) following $(1+1')$ resonance-enhanced multiphoton ionization (REMPI) in which the first photon prepares a single rovibrational level and the second photon ionizes that level provide us with an intimate probe of the ionization dynamics of molecules.[1-4] Our goal is to provide a theoretical expression that demonstrates how experimental results for PADs at various laser geometries are related to the magnitudes and phases of the radial dipole matrix elements that connect the intermediate state to the photoelectron partial waves. Using this expression, detailed dynamical information can be deduced from rotationally resolved PADs.

In our previous work on the $(1+1')$ REMPI of NO,[1] the excitation and ionization steps were carried out using two linearly polarized laser beams, and the resulting PADs were analyzed as though they had cylindrical symmetry. Here, we present an extension of our earlier work on breaking cylindrical symmetry.[5] We find that when the two linear polarization vectors are not parallel, the PADs are sensitive to coherences created in the intermediate state. Our formalism enables us to predict the resulting azimuthal dependence of the PAD and also the alignment of the "recoiling" ion. The sensitivity to coherences is analogous to that offered by the technique of laser-induced fluorescence.[6]

We consider an experiment such as that described in the following paper,[7] in which the two linearly polarized light beams have independently rotatable polarization vectors related by the Euler angles $\phi_T = 0°$, Θ_T, $\chi_T = 0°$. The geometry is illustrated in Fig. 1. When the polarization vectors are parallel ($\Theta_T = 0°$) the most straightforward situation results. Because the polarization vectors for excitation and ionization are collinear, cylindrical symmetry exists and the PAD is simply a function of θ, the angle between the polarization vector of the ionizing laser and the direction of the ejected photoelectron. Under these conditions, the PAD, $I(\theta,\phi)$, is given for a two-photon process by

$$I(\theta,\phi) = \beta_{00} Y_{00}(\theta,\phi) + \beta_{20} Y_{20}(\theta,\phi) + \beta_{40} Y_{40}(\theta,\phi)$$
$$= a_0[1 + a_2 P_2(\cos\theta) + a_4 P_4(\cos\theta)], \quad (1)$$

where the $Y_{LM}(\theta,\phi)$ are spherical harmonics and the $P_L(\cos\theta)$ are Legendre polynomials. The two are related by

$$P_L(\cos\theta) = [4\pi/(2L+1)]^{1/2} Y_{L0}(\theta,\phi). \quad (2)$$

Equation (1) is the form of typical one-color $(1+1)$ REMPI PADs.[8]

When $\Theta_T \neq 0°$, cylindrical symmetry is broken and the PAD becomes

$$I(\theta,\phi) = \beta_{00} Y_{00}(\theta,\phi) + \sum_{L=2,4} \sum_{M=-2}^{2} \beta_{LM} Y_{LM}(\theta,\phi). \quad (3)$$

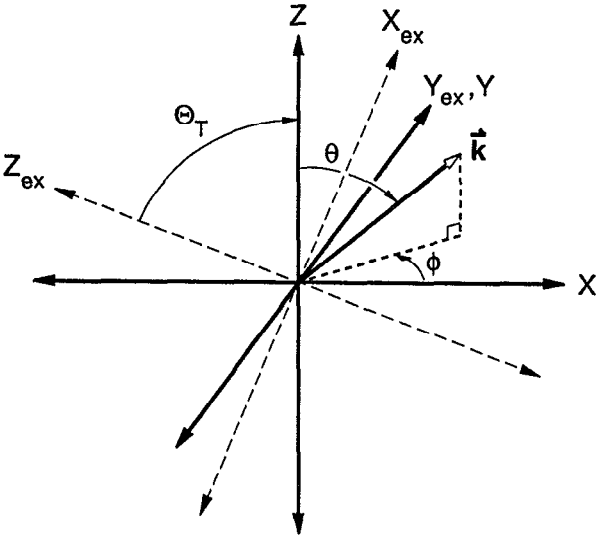

FIG. 1. Illustration of the axes and angles referred to in the text. The detector lies in the XZ plane ($\phi = 0°$), and the lasers propagate along the Y axis.

 0021-9606/91/151746-11$03.00

Because $I(\theta,\phi)$ is a real quantity, $\beta_{L2} = \beta_{L-2}$ and $\beta_{L1} = -\beta_{L-1}$. Hence, Eq. (3) reduces to

$$I(\theta,\phi) = \beta_{00} Y_{00}(\theta,\phi) + \sum_{L=2,4} \{\beta_{L0} Y_{L0}(\theta,\phi) + 2[\beta_{L1} Y_{L1}(\theta,0)\cos\phi + \beta_{L2} Y_{L2}(\theta,0)\cos 2\phi]\}, \quad (4)$$

which shows explicitly the ϕ dependence. In the special case of $\Theta_T = \pm 90°$, the β_{L1} terms vanish because reflection symmetry must be preserved. Thus, for this special case, $I(\theta,\phi) = I(-\theta,\phi)$ for any value of ϕ. In addition, when ϕ is equal to 90°, i.e., when the PAD is recorded in the YZ plane (see Fig. 1), there is reflection symmetry for any value of Θ_T.

We are able to probe the effects of both the "population alignment" [described by the state multipole $T(K,0)$] of M_{J_i} sublevels and the "coherence alignment" [described by the multipoles $T(K,Q \neq 0)$] between different M_{J_i} sublevels. (All quantum numbers are defined in Table I.) Both relative M_{J_i} populations and M_{J_i} coherence affect the θ dependence of the PAD. However, ϕ dependence and loss of reflection symmetry are brought about solely by the nonzero contributions of $Y_{2M}(\theta,\phi)$ and $Y_{4M}(\theta,\phi)$ with $M = \pm 1$ and ± 2, which results from coherence.[9,10]

The form of the PAD is determined by the β_{LM} coefficients. These coefficients can be related[11] to radial electric dipole matrix elements with magnitudes $r_{l\lambda}$ and overall phase shifts $\eta_{l\lambda}$ that connect the electronic wave function of the intermediate state to the outgoing partial waves. The radial dipole matrix elements can be expressed as follows:

$$r_{l\lambda} e^{i(\eta_{l\lambda} - \phi_{l\lambda})} = \int \chi^{+}_{\text{vib}}(R) \langle \Psi^{+}_{\text{elec}}(\{\mathbf{r}_s\};R) \Psi_{l\lambda}(\mathbf{k};R) \times \left| \sum_s r_s Y_{1\mu_\lambda}(\hat{\mathbf{r}}_s) \right| \Psi^{i}_{\text{elec}}(\{\mathbf{r}_s\};R) \rangle \chi^{i}_{\text{vib}}(R) dR, \quad (5)$$

where $\mu_\lambda = \Lambda^+ - \Lambda_i + \lambda$. The quantum numbers are defined in Table I, s labels the electrons in the intermediate state, R is the internuclear distance, $\mathbf{k}$ is the momentum vector of the electron moving in the direction (θ,ϕ), and $\phi_{l\lambda}$ is the scattering phase shift. Specifically, we will show that

$$\beta_{LM} = \sum_{ll'} \sum_{\lambda\lambda'} \sum_{m_l m'_l} \sqrt{\frac{(2l+1)(2l'+1)(2L+1)}{4\pi}} \times \begin{pmatrix} l & l' & L \\ m_l & -m'_l & M \end{pmatrix} \begin{pmatrix} l & l' & L \\ 0 & 0 & 0 \end{pmatrix} \times \gamma_{N^+ l\lambda m_l l'\lambda' m'_l}(\Theta_T) r_{l\lambda} r_{l'\lambda'} \cos(\eta_{l\lambda} - \eta_{l'\lambda'}), \quad (6)$$

where the $(:::)$ are Wigner 3-j symbols and the $\gamma_{N^+ l\lambda m_l l'\lambda' m'_l}(\Theta_T)$ are geometric factors whose values depend on the symmetry of the transition, the angular momentum coupling, and the angle between the two polarization vectors Θ_T. Hence, Eq. (6) relates the photoelectron angular distribution to the photoionization dynamics.

As shown in this paper, the form of the PAD may be predicted once the magnitudes of the radial dipole matrix elements, $r_{l\lambda}$, and the phase shift differences, $\eta_{l\lambda} - \eta_{l'\lambda'}$, are known. This prediction is achieved by calculating the $\gamma_{N^+ l\lambda m_l l'\lambda' m'_l}(\Theta_T)$ factors for the appropriate excitation–ionization geometry and then using Eqs. (6) and (4) to calculate the β_{LM} coefficients and the PAD, respectively. Conversely, Eq. (6) also enables us to deduce the dynamical parameters, $r_{l\lambda}$ and $\eta_{l\lambda} - \eta_{l'\lambda'}$, from experimental PADs once the $\gamma_{N^+ l\lambda m_l l'\lambda' m'_l}(\Theta_T)$ factors have been calculated (see following paper[7]).

In the next section, we derive an explicit formula for the $\gamma_{N^+ l\lambda m_l l'\lambda' m'_l}(\Theta_T)$ factors for an intermediate state described by Hund's case (b) coupling. In the Discussion, we present calculations on the $NO(X\,^2\Pi) \rightarrow NO(A\,^2\Sigma^+) \rightarrow NO^+(X\,^1\Sigma^+) + e^-$ system. Using the results of a nonlinear least-squares fit for the values of $r_{l\lambda}$ and $\eta_{l\lambda} - \eta_{l'\lambda'}$,[7] we predict the effect that the coherence terms have on the θ

TABLE I. Quantum numbers used in the text. Here, x may be subscript g, i, or superscript $+$, denoting ground, intermediate and ion state, respectively. It may also stand for the subscript t which denotes transferred angular momentum. The use of any quantity with a prime indicates a value coherently prepared with the unprimed value.

Angular momentum	Lab-fixed projection	Molecule-fixed projection	Description of angular momentum
J_x	M_{J_x}	Ω_x	Total angular momentum (excluding nuclear spin)
N_x	M_{N_x}	Λ_x	Nuclear rotation plus orbital angular momentum
S_x	M_{S_x}	Σ_x	Total electronic spin
l	m_l	λ	Photoelectron orbital angular momentum
1	μ,μ_0[a]	μ_λ	Photon angular momentum
L	M		Rank of the l spherical tensor
K	Q		Rank of the N_i spherical tensor
K^+	Q^+		Rank of the N^+ spherical tensor

[a] μ refers to a projection in the excitation frame and μ_0 to a projection in the ionization frame.

and ϕ dependence of PADs involving the transitions $R_{21}(1.5)$ and $Q_1(2.5)$ for $\Theta_T = 0°$, 54.7°, and 90°. We note that the transition $Q_1(2.5)$ cannot be resolved from the transition $P_{21}(2.5)$ in an experiment such as that described in the following paper but it provides an interesting illustration. We also discuss the alignment of the ion in each rotational state.

II. THEORY

In this section we derive the expression for the $\gamma_{N^+ l\lambda m_l l'\lambda' m_l'}(\Theta_T)$ factors that appear in Eq. (6) and hence the β_{LM} coefficients when a single rotational level is photoionized. We are most interested in the $\beta_{LM\neq 0}$ coefficients because nonzero values of these coefficients correspond to broken cylindrical symmetry and hence ϕ dependent and skewed PADs. From Eq. (6) we see that nonzero values of such coefficients arise when $m_l \neq m_l'$, that is, from interference terms. These terms occur as a result of coherently preparing M_{J_i} sublevels in the intermediate state. Consequently they are absent when only one possible route connects a given M_{J_g} to a given M_{J^+}. Such is the case when the projection of the photon angular momentum is well defined in a common laboratory frame for the excitation and ionization steps. Following other workers in the field,[1,11] we treat the bound–bound transition to the intermediate state and the bound–free transition from the intermediate state to the ionization continuum as two steps. We consider both processes in the "ionization frame," as opposed to the "excitation frame," i.e., the laboratory Z axis is chosen to lie along the polarization vector of the ionizing radiation (see Fig. 1). At the end of this section, we present the equations necessary to calculate the ion alignment for each rotational state.

A. Intermediate state

Use of a density matrix formalism to describe the M_{J_i} distribution following excitation is most appropriate[11,12] because it represents both population and coherence terms in one expression.[13] The former are represented by diagonal elements ($M_{J_i} = M_{J_i}'$) and the latter by off-diagonal elements ($M_{J_i} \neq M_{J_i}'$). For our purposes, considering the M_{J_i} distribution to be time independent (weak-field approximation) suffices. We assume that (a) Zeeman and Stark splittings are absent because the experiment is performed under field-free conditions in a weak radiation field, and (b) the presence of hyperfine structure (which can cause depolarization in time) can be neglected because nanosecond laser pulses are used.

The density matrix reflects the population, the alignment, and the coherences in the intermediate state. When the laser polarizations are parallel ($\Theta_T = 0°$), the coherence terms (off-diagonal elements) are zero and the density matrix simply denotes the population, $T(0,0)$, and the "population alignment," $T(2,0)$. In this case, the density matrix is diagonal and can be written as follows:

$$ {}^{J_i}\rho_{M_{J_i}M_{J_i}}(\Theta_T = 0°) \propto S(J_g,J_i) \sum_{M_{J_g}} \begin{pmatrix} J_g & 1 & J_i \\ -M_{J_g} & \mu_0 & M_{J_i} \end{pmatrix}^2, \tag{7} $$

where $S(J_g,J_i)$ is the rotational linestrength connecting the ground and intermediate state rotational levels, and the 3-j symbol expresses the alignment. Here, μ_0 is the well-defined projection of the photon angular momentum on the Z axis (equal to 0 for linearly polarized light).

When $\Theta_T \neq 0°$, a rotation is introduced between the excitation and ionization frames. Formally, this rotation is performed by rotation matrix elements that transform the photon projection μ_0 in the excitation frame to the projection μ in the ionization frame where μ can be 1, 0, or -1. In other words, the photon is described by a linear superposition of all possible projections following this frame transformation. The values M_{J_i} and M_{J_i}' that result from connecting M_{J_g} with μ and μ', respectively, are coherently prepared. Therefore, an off-diagonal element exists that connects the two.

Thus, we write the density matrix elements in the ionization frame as follows:[14]

$$ \begin{aligned} &{}^{J_i}\rho_{M_{J_i}M_{J_i}'}(\Theta_T) \\ &\quad \propto S(J_g,J_i) \sum_{\mu\mu'} \sum_{M_{J_g}} (-1)^{2J_i + M_{J_i} + M_{J_i}'} \\ &\qquad \times D^{1*}_{\mu_0\mu}(0,\Theta_T,0) D^{1}_{\mu_0\mu'}(0,\Theta_T,0) \\ &\qquad \times \begin{pmatrix} J_g & 1 & J_i \\ -M_{J_g} & \mu & M_{J_i} \end{pmatrix} \begin{pmatrix} J_g & 1 & J_i \\ -M_{J_g} & \mu' & M_{J_i}' \end{pmatrix}, \end{aligned} \tag{8} $$

which is a valid expression for all Θ_T. Note that Eq. (8) reduces to Eq. (7) when $\Theta_T = 0°$.

While Eqs. (7) and (8) are valid for both Hund's case (a) and Hund's case (b) wave functions, we consider an intermediate state wave function well described by Hund's case (b). In case (b), spin functions are uncoupled and therefore we write the density matrix in terms of the quantum number N instead of J. The two representations can be related as follows:

$$ \begin{aligned} &{}^{N_i}\rho_{M_{N_i}M_{N_i}'}(\Theta_T) \\ &\quad = \sum_{J_i M_{S_i}} \sum_{M_{J_i} M_{J_i}'} {}^{J_i}\rho_{M_{J_i}M_{J_i}'}(\Theta_T) (-1)^{M_{N_i} + M_{N_i}'} \\ &\qquad \times \begin{pmatrix} J_i & N_i & S_i \\ -M_{J_i} & M_{N_i} & M_{S_i} \end{pmatrix} \begin{pmatrix} J_i & N_i & S_i \\ -M_{J_i}' & M_{N_i}' & M_{S_i} \end{pmatrix}. \end{aligned} \tag{9} $$

An apt way of illustrating the importance of coherence terms is to recast the density matrix into spherical tensors called state multipoles,[13,15]

$$ \begin{aligned} &T(K,Q;\Theta_T) \\ &\quad = \sum_{M_{N_i} M_{N_i}'} (-1)^{N_i - M_{N_i}} (2K+1)^{1/2} \\ &\qquad \times \begin{pmatrix} N_i & N_i & K \\ M_{N_i} & -M_{N_i}' & Q \end{pmatrix} {}^{N_i}\rho_{M_{N_i}M_{N_i}'}(\Theta_T). \end{aligned} \tag{10} $$

Here, K and Q are the rank and component of the spherical tensor T. Henceforward, for simplicity, we omit the Θ_T argument of the multipoles. Thus, $T(0,0)$ represents the popu-

lation of the M_{N_i} sublevels. The quadrupole tensor $T(2,Q)$ represents alignment. When the component Q is nonzero, the $T(2,Q)$ represent coherence terms. The degree of coherence depends on the frame in which we calculate the density matrix and is determined by Θ_T.

As a simple illustration, we take the case of a Q branch transition between two electronic doublet states. In Table II we display for the transition $Q_1(2.5)$ the density matrices and state multipoles that describe the M_{N_i} distribution in the intermediate state for three excitation–ionization geometries; $\Theta_T = 0°$, $\Theta_T = 54.7°$, and $\Theta_T = 90°$. We note that each of these geometries is a special case because at least one of the $T(2,Q)$ multipoles is zero.

B. Ionization step

In our notation, the intermediate state is described by $|\alpha_i N_i \Lambda_i M_{N_i} S_i\rangle$ and the ion + photoelectron by $|\alpha^+ N^+ \Lambda^+ M_{N^+} S^+; \mathbf{k}, l\lambda m_l\rangle$ where α denotes all other quantum numbers required to specify each state. The matrix element for the ionization step is derived in Appendix A for ionization with linearly polarized light ($\mu_0 = 0$). Summing Eq. (A6) over μ_λ yields

$$\langle \alpha^+ N^+ \Lambda^+ M_{N^+} S^+; \mathbf{k}, l\lambda m_l | D(1,\mu_0 = 0) | \alpha_i N_i \Lambda_i M_{N_i} S_i \rangle$$
$$= \sqrt{(2N_i + 1)(2N^+ + 1)} \sum_{N_t \mu_\lambda} (-1)^{M_{N^+} + \Lambda^+ + \mu_\lambda} (2N_t + 1)(-i)^l e^{i\eta_{l\lambda}} r_{l\lambda} Y_{lm_l}(\theta,\phi)$$
$$\times \begin{pmatrix} N_t & 1 & l \\ M_{N_t} & 0 & m_l \end{pmatrix} \begin{pmatrix} N^+ & N_i & N_t \\ -\Lambda^+ & \Lambda_i & \Lambda_t \end{pmatrix} \begin{pmatrix} N_t & 1 & l \\ -\Lambda_t & \mu_\lambda & -\lambda \end{pmatrix} \begin{pmatrix} N^+ & N_i & N_t \\ -M_{N^+} & M_{N_i} & M_{N_t} \end{pmatrix}, \tag{11}$$

where $D(1,\mu_0)$ is the electric dipole operator. This result is similar to that of Dixit and McKoy.[11] Because N is taken to be a good quantum number, this expression is most appropriate for intermediate and ion states well described by Hund's case (b) wave functions. Additionally, both spin–orbit coupling and spin–rotation coupling are assumed to be negligible and so the spin part of the matrix element can be separated out without affecting the result. This separation is applicable to both case (a) and case (b) wave functions but not to case (c). The role of spin–orbit coupling in photoionization is being considered in greater depth.[16] Equation (11) can be easily extended to case (a) wave functions by expressing them as an expansion in a basis set of Hund's case (b) wave functions.

To find the probability of detecting the final state $|\alpha^+ N^+ \Lambda^+ M_{N^+} S^+; \mathbf{k}, l\lambda m_l\rangle$ in the solid angle element $d\Omega = \sin\theta d\theta d\phi$, Eq. (11) must be squared. Correct performance of this operation requires knowledge of which quantum states can interfere. When $\Theta_T = 0°$ there is no M_{J_i} coherence (and thus no M_{N_i} coherence) in the intermediate state, and only ionization channels involving different values of l, λ, μ_λ, and N_t can interfere. When $\Theta_T \neq 0°$, however, the *laboratory frame* sublevels $M_{J_i} = M_{J_g}$, $M_{J_g} \pm 1$ may have originated from the same sublevel, M_{J_g}. By the same token, more than one M_{N_i} will also have originated from the same M_{J_g}. As a result, remembering that spin is a spectator in this ionization process, the sublevel M_{N^+} can be reached from M_{J_g} by routes involving more than one M_{N_i} with corresponding values of m_l. Consequently, these M_{N_i} and m_l values must be allowed to interfere. This concept is illustrated in Fig. 2 for the simple case of a $Q_1(2.5)$, $M_{J_g} = -1/2 \rightarrow M_{N^+} = 0$ transition for a value of Θ_T other than 0° or 90°.

We obtain for the square of Eq. (11)

TABLE II. Density matrices and state multipoles for the intermediate level, $N_i = 2$, following the transition $Q_1(2.5)$, for three different laser geometries described by the angle Θ_T. The multipoles for $K > 0$ are divided by $T(0,0)$ for each Θ_T value.

		M'_{N_i}					
Θ_T	M_{N_i}	−2	−1	0	1	2	$T(K,Q)$
0°	−2	0.383	0.0	0.0	0.0	0.0	$T(0,0) = 0.447$
	−1	0.0	0.109	0.0	0.0	0.0	$T(2,0) = 0.765$
	0	0.0	0.0	0.017	0.0	0.0	
	1	0.0	0.0	0.0	0.109	0.0	
	2	0.0	0.0	0.0	0.0	0.383	
90°	−2	0.109	0.0	0.112	0.0	0.0	$T(0,0) = 0.447$
	−1	0.0	0.245	0.0	0.137	0.0	$T(2,0) = -0.382$
	0	0.112	0.0	0.291	0.0	0.112	$T(2,\pm 2) = 0.468$
	1	0.0	0.137	0.0	0.245	0.0	
	2	0.0	0.0	0.112	0.0	0.109	
54.7°	−2	0.200	0.129	0.075	0.0	0.0	$T(0,0) = 0.447$
	−1	0.129	0.200	0.053	0.091	0.0	$T(2,0) = 0.0$
	0	0.075	0.053	0.200	−0.053	0.075	$T(2,\pm 1) = \mp 0.442$
	1	0.0	0.091	−0.053	0.200	−0.129	$T(2,\pm 2) = 0.312$
	2	0.0	0.0	0.075	−0.129	0.200	

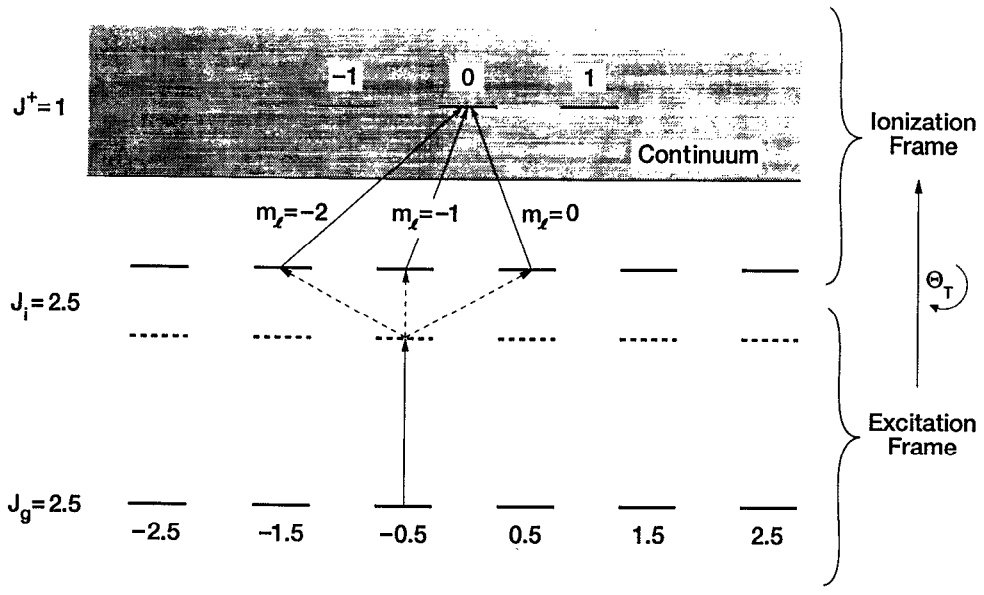

FIG. 2. Illustration of interfering ionization channels when the excitation–ionization geometry is described by Θ_T.

$$\langle \alpha^+ N^+ \Lambda^+ M_{N^+} S^+;\mathbf{k},l'm_l'\lambda' | D(1,0) | \alpha_i N_i \Lambda_i M'_{N_i} S_i \rangle \langle \alpha_i N_i \Lambda_i M_{N_i} S_i | D^*(1,0) | \alpha^+ N^+ \Lambda^+ M_{N^+} S^+;\mathbf{k},lm_l\lambda \rangle$$

$$= (2N_i+1)(2N^++1) \sum_{N_t N'_t} \sum_{\mu_\lambda \mu'_\lambda} C(l'\lambda' m'_l N'_t M'_{N_t} \mu'_\lambda) C(l\lambda m_l N_t M_{N_t} \mu_\lambda)$$

$$\times Y_{lm_l}(\theta,\phi) Y^*_{l'm'_l}(\theta,\phi) (-i)^{l'-l} e^{i(\eta_{l\lambda} - \eta_{l'\lambda'})} r_{l\lambda} r_{l'\lambda'}, \tag{12}$$

where

$$C(l\lambda m_l N_t M_{N_t} \mu_\lambda) = (2N_t+1)(-1)^{M_{N^+}+\mu_\lambda} \begin{pmatrix} N_t & 1 & l \\ M_{N_t} & 0 & m_l \end{pmatrix}$$

$$\times \begin{pmatrix} N^+ & N_i & N_t \\ -\Lambda^+ & \Lambda_i & \Lambda_t \end{pmatrix} \begin{pmatrix} N_t & 1 & l \\ -\Lambda_t & \mu_\lambda & -\lambda \end{pmatrix} \begin{pmatrix} N^+ & N_i & N_t \\ -M_{N^+} & M_{N_i} & M_{N_t} \end{pmatrix} \tag{13}$$

and, for this $(1+1')$ REMPI process, $|m'_l - m_l| = |M'_{N_t} - M_{N_t}| \leqslant 2$. Thus, we can write the intensity of photoelectrons detected in the solid angle element $d\Omega = \sin\theta d\theta d\phi$ associated with a final state rotational level N^+ and for an excitation-ionization geometry described by Θ_T as

$$I(\theta,\phi) = \sum_{M_{N^+}} \sum_{M_{N_i} M'_{N_i}} \sum_{ll'} \sum_{\lambda\lambda'} \sum_{m_l m'_l} \langle \alpha^+ N^+ \Lambda^+ M_{N^+} S^+; \quad \mathbf{k},l'm'_l\lambda' | D(1,0) | \alpha_i N_i \Lambda_i M'_{N_i} S_i \rangle$$

$$\times \langle \alpha_i N_i \Lambda_i M_{N_i} S_i | D^*(1,0) | \alpha^+ N^+ \Lambda^+ M_{N^+} S^+; \quad \mathbf{k},lm_l\lambda \rangle^{N_i} \rho_{M_{N_i} M'_{N_i}}(\Theta_T)$$

$$= \sum_{ll'} \sum_{\lambda\lambda'} \sum_{m_l m'_l} \gamma_{N^+ l\lambda m_l l'\lambda' m'_l}(\Theta_T) r_{l\lambda} r_{l'\lambda'} \cos(\eta_{l\lambda} - \eta_{l'\lambda'}) Y_{lm_l}(\theta,\phi) Y^*_{l'm'_l}(\theta,\phi), \tag{14}$$

where

$$\gamma_{N^+ l\lambda m_l l'\lambda' m'_l}(\Theta_T)$$

$$= (2N_i+1)(2N^++1)(-i)^{l'-l}$$

$$\times \sum_{M_{N^+}} \sum_{M_{N_i} M'_{N_i}} \sum_{N_i N'_i} \sum_{\mu_\lambda \mu'_\lambda} {}^{N_i}\rho_{M_{N_i} M'_{N_i}}(\Theta_T)$$

$$\times C(l'\lambda' m'_l N'_t M'_{N_t} \mu'_\lambda) C(l\lambda m_l N_t M_{N_t} \mu_\lambda). \tag{15}$$

Because

$$I(\theta,\phi) = \beta_{00} Y_{00}(\theta,\phi) + \sum_{L=2,4} \sum_{M=-2} \beta_{LM} Y_{LM}(\theta,\phi), \tag{16}$$

it follows from Eq. (12) that

$$\beta_{LM} = \sum_{ll'} \sum_{\lambda\lambda'} \sum_{m_l m'_l} \sqrt{\frac{(2l+1)(2l'+1)(2L+1)}{4\pi}}$$

$$\times \begin{pmatrix} l & l' & L \\ m_l & -m'_l & M \end{pmatrix} \begin{pmatrix} l & l' & L \\ 0 & 0 & 0 \end{pmatrix}$$

$$\times \gamma_{N^+ l\lambda m_l l'\lambda' m'_l}(\Theta_T) r_{l\lambda} r_{l'\lambda'} \cos(\eta_{l\lambda} - \eta_{l'\lambda'}), \tag{17}$$

which is seen to be identical to Eq. (6).

We identify L and M with the rank and component of the spherical tensor for the photoelectron m_l distribution. For example, β_{00} gives the angle-integrated cross section for the (J_g,N^+) branch in question. The second photon can increase the rank of the distribution so that where $K=0,2$ for the intermediate state multipole, we have $L=0,2,4$. However, the component M is unchanged on ionization (i.e., $M=Q$) because, with the choice of the Z axis to be along the electric vector of the ionizing photon, all the noncylindrical character is introduced in the excitation step.

In other words, the terms with $M\neq 0$ appear only when there are nonzero values of the $T(K,Q=M)$ that represent the intermediate state. These terms are therefore a result of M_{N_i} (and hence m_l) coherence and give rise to an azimuthal dependence of the angular distribution that is dependent on powers of $\cos\phi$. In addition, when $Q=\pm 1$, they can cause the appearance of a skewed angular distribution.

C. Ion alignment

Further use may be made of our formalism in deducing an expression for the alignment of the ion from which a photoelectron was ejected. To make this deduction, we integrate Eq. (12) over θ and ϕ and omit the sum over M_{N^+} in Eq. (15). From the integration we obtain the elements of the density matrix for the ion in the rotational level N^+,

$$
\begin{aligned}
&{}^{N^+}\rho_{M_{N^+}M'_{N^+}}(\Theta_T)\\
&\quad=\sum_l\sum_{m_l}\sum_{\lambda\lambda'}\frac{(-1)^{m_l}}{\sqrt{4\pi}}\gamma'_{N^+M_{N^+}M'_{N^+}lm_l\lambda\lambda'}(\Theta_T)\\
&\qquad\times r_{l\lambda}r_{l\lambda'}\cos(\eta_{l\lambda}-\eta_{l\lambda'}),
\end{aligned}
\tag{18}
$$

where

$$
\begin{aligned}
&\gamma'_{N^+M_{N^+}M'_{N^+}lm_l\lambda\lambda'}(\Theta_T)\\
&\quad=(2N_i+1)(2N^++1)\\
&\qquad\times\sum_{M_{N_i}M'_{N_i}}\sum_{N_iN'_i}\sum_{\mu_\lambda\mu'_\lambda}{}^{N_i}\rho_{M_{N_i}M'_{N_i}}(\Theta_T)(2N_i+1)\\
&\qquad\times C(N'_iM'_{N_i}M'_{N^+}\mu'_\lambda\lambda')C(N_iM_{N_i}M_{N^+}\mu_\lambda\lambda).
\end{aligned}
\tag{19}
$$

In Eq. (19), the coefficient C is the same as in Eq. (13) but has been labeled with new coherent quantities as we explain. A result of the integration is that interference terms between different values of l and m_l vanish (i.e., $l=l'$ and $m_l=m'_l$). This disappearance occurs because the measurement of the alignment of the ion in the rotational level N^+ is in a sense an observation of M_{N^+}. As a consequence, we must treat interference between routes that connect common values of M_{J_g} and m_l. Thus, we must consider interfering values of M_N. (off-diagonal elements in the density matrix for the ion). Conversely, when we observe PADs (and thus l and m_l), we consider paths that connect common values of M_{J_g} and M_{N^+}, which results in interfering values of l and m_l. As can be seen in Eq. (18) however, λ interference, unlike l or m_l interference, *does* affect the ion alignment. This λ interference is an important factor in determining ion rotational branching ratios as has been observed experimentally.[1,7]

We can express the rotational state multipoles of the ion as in Eq. (10),

$$
\begin{aligned}
T(K^+,Q^+)=&\sum_{M_{N^+}M'_{N^+}}(-1)^{N^+-M_{N^+}}\\
&\times\begin{pmatrix}N^+ & N^+ & K^+\\ M_{N^+} & -M'_{N^+} & Q^+\end{pmatrix}\\
&\times\sqrt{(2K^++1)}\,{}^{N^+}\rho_{M_{N^+}M'_{N^+}}(\Theta_T).
\end{aligned}
\tag{20}
$$

Therefore, if the magnitudes and phases of the radial dipole matrix elements are known, the alignment of the different final rotational levels of the ion can be predicted. Because these dynamical quantities can be deduced from the measurement of rotationally resolved PADs, all the information required to calculate the alignment of a rotational level of the ion can be obtained from such angle- and energy-resolved photoelectron measurements.

III. DISCUSSION

We have presented a general expression for the photoelectron angular distribution following two consecutive electric dipole transitions in a rotating molecule, each with linearly polarized light. We find that when the two polarization vectors make a nonzero angle Θ_T, cylindrical symmetry of the excitation–ionization process is broken. This result has the consequence of making the PAD sensitive to coherences in the intermediate state and hence showing a ϕ dependence. Moreover, for $\phi\neq 90°$, the θ dependence does not have reflection symmetry, i.e., the PAD is skewed. This effect is maximized at $\phi=0°$. A special case is $\Theta_T=\pm 90°$, in which reflection symmetry is preserved for any value of ϕ.

Other work that was concerned with the effect of polarization on REMPI-PADs has been performed mostly on atoms. For comprehensive reviews of these, the reader is referred to Leuchs and Walther[9] and Smith and Leuchs.[10] Pioneering work was carried out by Berry's group[17,18] who observed skewed angular distributions following two-photon ionization of alkali and alkaline earth metal atoms when the two polarization vectors were at a number of angles.[18] The earliest observation of a complete ϕ dependence was made by Smith *et al.*[19] who investigated the role of quadrupole transitions in atomic photoionization. An interesting result is the recent observation of skewed angular distributions following above-threshold ionization (ATI) with elliptically polarized light.[20] This observation is a singular example of PADs having lower symmetry than the combination of the exciting and ionizing radiation.

Theoretical work in the groups of Berry and McKoy has addressed the role of polarization in REMPI-PADs of molecules when the polarization of the ionizing photon is linear[21] and circular.[22] In the work most relevant to this paper, Berry and co-workers predicted the effect of broken cylindrical symmetry on nonrotationally resolved PADs. The calculations of McKoy and co-workers illustrate the effects of circular dichroism in PADs which occur because the PADs are skewed. This effect has been observed experimentally.[23] We are not aware of any experimental work besides ours[1,7] that

examines the effect of varying the angle between linear polarization vectors on rotationally resolved REMPI-PADs in molecules.

In this paper, we have provided a general description of molecular PADs that includes $Y_{L,M\neq 0}(\theta,\phi)$ terms. We demonstrate, moreover, that these terms have a significant effect on such PADs. To illustrate this effect, we consider the $(1+1')$ REMPI process $NO(X\,^2\Pi)\rightarrow NO(A\,^2\Sigma^+)\rightarrow NO^+(X\,^1\Sigma^+)+e^-$ as an example. We choose this system because it is readily investigated experimentally (see following paper[7]). For this system, we have made quantitative predictions of the effect of intermediate state coherences on PADs. Because the intermediate and ion states both have Σ symmetry in this example, $\Lambda^+=\Lambda_i=0$, which simplifies Eq. (11).

We calculate the γ factors [Eq. (15)] for the photoionization of an intermediate level prepared by the transitions $R_{21}(1.5)$ and $Q_1(2.5)$ at the three geometries, $\Theta_T=0°$, 54.7°, and 90°. To calculate the β_{LM} values [Eq. (17)] and hence PADs, we need values for the magnitudes of the radial dipole matrix elements and the phase differences ($r_{l\lambda}$ and $\eta_{l\lambda}-\eta_{l'\lambda'}$). Here, we use the results of a fit to the experimental data presented in the following paper.[7] β_{LM} values for photoionization via the Q branch transition are presented in Table III. The resulting PADs are illustrated in Figs. 3–7.

Figure 3 shows results for the $R_{21}(1.5)$ and $Q_1(2.5)$ transitions for each ΔN ($=N^+-N_i$) at $\Theta_T=0°$. In an experiment such as that described in the following paper,[7] it would not be possible to resolve the ΔN levels for such a low value of N_i. However, these results provide an interesting illustration of a qualitative effect that remains at higher N_i. As noted before,[1] we see a strong dependence on both branch and ion rotational state which demonstrates the importance

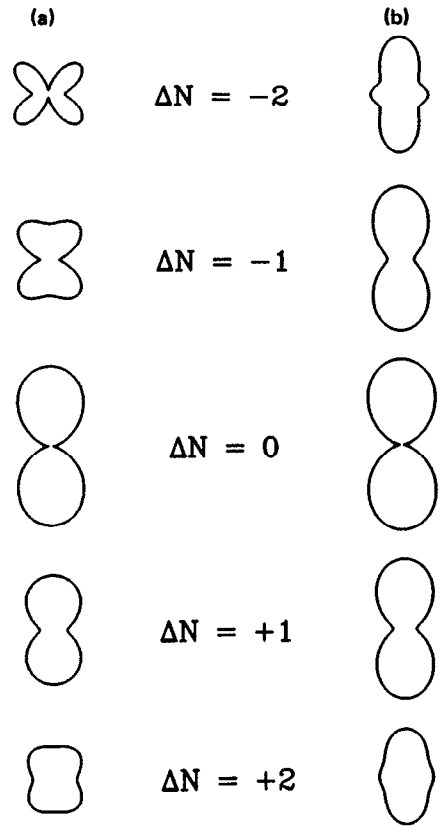

FIG. 3. Predicted photoelectron angular distributions (PADs) for $\Theta_T=0°$, at any fixed value of ϕ, using the dynamical parameters presented in the following paper (Ref. 7). Ionization follows the ground-to-intermediate transitions (a) $Q_1(2.5)$ and (b) $R_{21}(1.5)$. ΔN denotes the change in rotational angular momentum between the intermediate and the ion ($\Delta N=N^+-N_i$).

TABLE III. Predictions of β_{LM} values describing the PADs following the transition $Q_1(2.5)$ for three geometries. These values are calculated using the dynamical parameters deduced in the following paper.[7] The $\beta_{L>0,M}$ values are divided by β_{00} for each N^+, Θ_T combination. The β_{00} values are normalized such that $\beta_{00}\equiv 100$ for $\Theta_T=0°$, $\Delta N=0$ ($N^+=2$).

		N^+				
Θ_T	β_{LM}	0	1	2	3	4
0°	β_{00}	5.015	2.216	≡100	4.726	13.796
	β_{20}	0.076	0.464	0.823	0.616	0.144
	β_{40}	−0.340	−0.212	−0.005	−0.045	−0.095
90°	β_{00}	6.788	4.876	100.805	6.193	17.176
	β_{20}	0.224	0.761	0.835	0.777	0.199
	$\beta_{2\pm2}$	−0.268	−0.062	0.003	−0.014	−0.060
	β_{40}	0.126	0.048	0.002	0.017	0.038
	$\beta_{4\pm2}$	−0.099	−0.038	−0.002	−0.013	−0.030
54.7°	β_{00}	6.197	3.977	100.540	5.704	16.049
	β_{20}	0.184	0.706	0.831	0.732	0.184
	$\beta_{2\pm1}$	∓0.122	∓0.211	∓0.005	∓0.100	∓0.041
	$\beta_{2\pm2}$	−0.195	−0.050	0.002	−0.010	−0.043
	β_{40}	0	0	0	0	0
	$\beta_{4\pm1}$	∓0.145	∓0.062	∓0.003	∓0.019	∓0.043
	$\beta_{4\pm2}$	−0.073	−0.031	−0.001	−0.010	−0.022

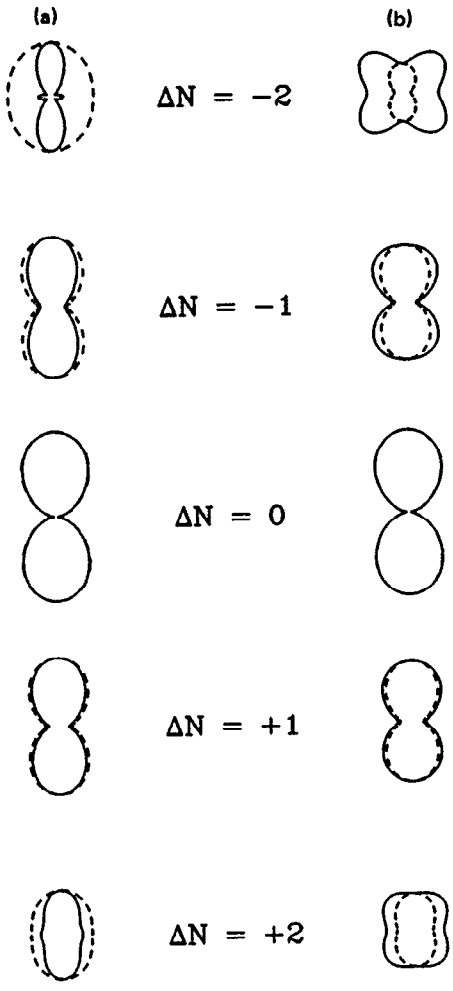

FIG. 4. Illustration of the ϕ dependence of PADs when $\Theta_T = 90°$. The solid line indicates the predicted θ dependence for $\phi = 0°$, and the dashed line indicates the predicted θ dependence for $\phi = 90°$. Ionization follows the ground-to-intermediate transitions (a) $Q_1(2.5)$ and (b) $R_{21}(1.5)$.

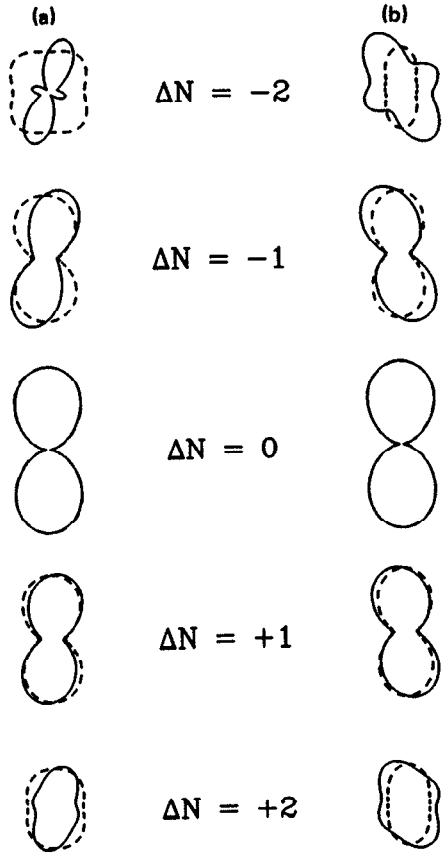

FIG. 5. Illustration of the ϕ dependence of PADs when $\Theta_T = 54.7°$. The solid line indicates the predicted θ dependence for $\phi = 0°$, and the dashed line indicates the predicted θ dependence for $\phi = 90°$. Ionization follows the ground-to-intermediate transitions (a) $Q_1(2.5)$ and (b) $R_{21}(1.5)$.

of ion rotational state resolution. In addition, we note the marked $\Delta N = \pm 2$ PAD asymmetry. This asymmetry results from choosing low values of J_i. When the ion has no rotational angular momentum it can have no alignment and all anisotropy must show up in the photoelectron angular distribution. This asymmetry is also seen in the calculations of Rudolph *et al.*[24] for the transitions $P_{21}(J_i)$ where $J_i = 1.5 \rightarrow 4.5$. At high J_i, the model predicts equivalent $\Delta N = \pm 2$ PADs.

Figures 4 and 5 show the θ dependence of PADs for two fixed values of ϕ. We see that the contributions from the $Y_{2,M\neq 0}(\theta,\phi)$ and $Y_{4,M\neq 0}(\theta,\phi)$ terms to the PADs are most dramatic for $\Delta N = \pm 2$; the shape at $\phi = 90°$ is quite different from that at $\phi = 0°$. Another striking feature is the skewed angular distributions seen in Fig. 5. These occur for any Θ_T values other than 0° or 90° and result from the presence of the $Y_{L\pm 1}(\theta,\phi)$ terms. The fact that no skewing occurs for the $\Delta N = 0$ PAD in Fig. 5 is important because it is a dynamical effect. The $p\lambda$ waves dominate the $\Delta N = 0$ transition; if we choose different values for the $\eta_{p\sigma} - \eta_{p\pi}$ relative phase shift, then this PAD can become skewed, as illustrated in Fig. 6.

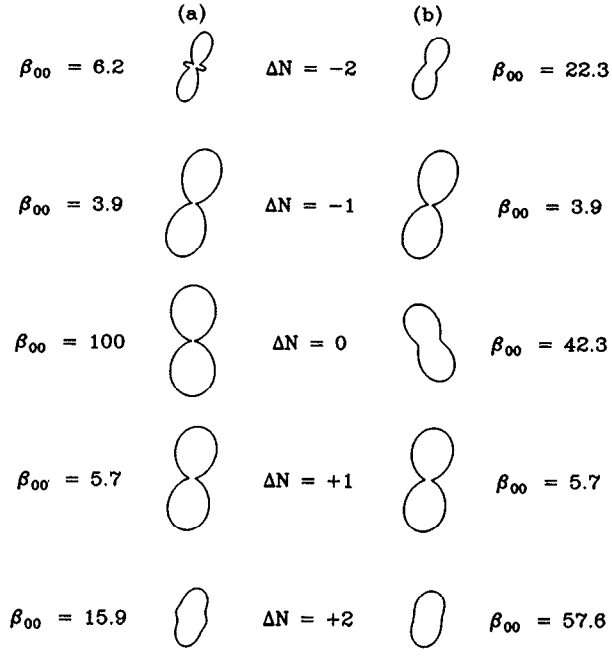

FIG. 6. Illustration of the effect of changing the relative phase, $\eta_{p\sigma} - \eta_{p\pi}$. Both (a) and (b) show predicted PADs following the ground-to-intermediate transition $Q_1(2.5)$ for the excitation–ionization geometry $\Theta_T = 54.7°$ with $\phi = 0°$. In (a) the PAD was calculated using the $\eta_{p\sigma} - \eta_{p\pi}$ phase presented in the following paper (Ref. 7), and in (b) the PAD was calculated using a $\eta_{p\sigma} - \eta_{p\pi}$ phase different by π radians.

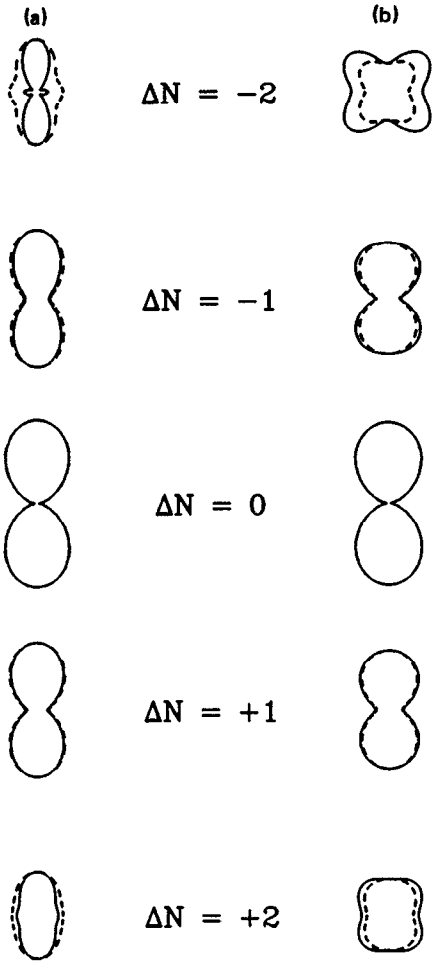

FIG. 7. Illustration of the effect of omitting coherence terms on PADs for the excitation–ionization geometry $\Theta_T = 90°$ for $\phi = 0°$. The solid line indicates PADs with coherence terms included (correct) and the dashed line indicates PADs with coherence terms omitted (incorrect). Ionization follows the ground-to-intermediate transitions (a) $Q_1(2.5)$ and (b) $R_{21}(1.5)$.

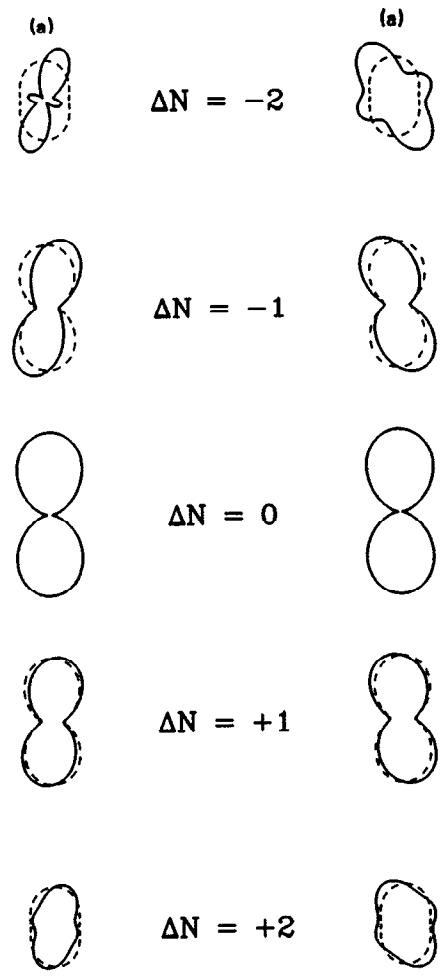

FIG. 8. Illustration of the effect of omitting coherence terms on PADs for the excitation–ionization geometry $\Theta_T = 54.7°$ for $\phi = 0°$. The solid line indicates PADs with coherence terms included (correct) and the dashed line indicates PADs with coherence terms omitted (incorrect). The ground-to-intermediate transitions are (a) $Q_1(2.5)$ and (b) $R_{21}(1.5)$.

For any value of ϕ, the $Y_{2,M\neq 0}(\theta,\phi)$ and $Y_{4,M\neq 0}(\theta,\phi)$ terms have a significant effect on the θ dependence of the PADs. In Fig. 7 we show the calculated PADs for $\Theta_T = 90°$, $\phi = 0°$ with (a) coherence terms included and (b) coherence terms omitted. We show the same in Fig. 8 for $\Theta_T = 54.7°$. Note that by omitting coherence terms, much of the anisotropy in the PADs is washed out and that in fact we see a ϕ-averaged result.

An especially interesting case arises when $\Theta_T = 54.7°$, the so-called magic angle. Here, the intermediate state has $T(2,0) = 0$, i.e., there is no population alignment in the ionizing frame. However, we cannot describe the PADs by the familiar expression[25]

$$I(\theta,\phi) = I(\theta) = \alpha[1 + \beta P_2(\cos\theta)]$$
$$= \beta_{00} Y_{00}(\theta,0) + \beta_{20} Y_{20}(\theta,0) \qquad (21)$$

because of the presence of the coherence terms, $T(K,Q \neq 0)$. These terms give rise to additional $Y_{LM}(\theta,\phi)$ contributions to the PAD. [Of course, if a truly unaligned intermediate state were ionized, Eq. (21) would suffice.] We also note that, as for other nonzero, non-90° angles, there is no reflection symmetry $[I(\theta,\phi) \neq I(-\theta,\phi)]$ when $\phi \neq 90°$. This lack of symmetry indicates that the excitation and ionization processes are weighted differently. As shown in the following paper, $\Theta_T = +54.7°$ gives rise to the opposite PAD skew from $\Theta_T = -54.7°$. The PADs for $\Theta_T = \pm 54.7°$ at $\phi = 0°$ provide a good test of the importance of coherence terms because any deviation from Eq. (21) is an indication of coherence that is independent of any model or fit. Also, any skewing is qualitatively obvious.

Another interesting illustration of the effect of coherence terms would be to measure PADs for $\Theta_T \neq 0°$ at more than one value of ϕ as the predictions shown in Figs. 4 and 5 suggest. In the experiment we discuss here, this measurement would be a direct indication of the effect of coherence because any deviation from cylindrical symmetry arises from these terms. Unfortunately, such a measurement is experimentally difficult.

As shown in Sec. II C, our formalism also provides us with a simple means of deducing the alignment of each rota-

TABLE IV. State multipoles $T(K^+,Q^+)$ describing the ion alignment when photoelectrons are ejected following the transition $Q_1(2.5)$ for three laser geometries. The multipoles for $K>0$ are divided by $T(0,0)$ for each N^+,Θ_I combination. The $T(0,0)$ are normalized such that $T(0,0)\equiv 100$ for $\Theta_T=0°$, $\Delta N=0$ $(N^+=2)$.

		N^+				
Θ_I	$T(K^+,Q^+)$	0	1	2	3	4
0°	$T(0,0)$	11.213	2.869	≡100	3.994	10.283
	$T(2,0)$	0.000	0.225	0.695	−0.012	0.367
	$T(4,0)$	0.000	0.000	−0.012	−0.502	−0.155
90°	$T(0,0)$	15.178	6.295	100.806	5.234	12.802
	$T(2,0)$	0.000	−0.385	−0.355	−0.649	−0.457
	$T(2,\pm 2)$	0.000	0.209	0.407	0.346	0.342
	$T(4,0)$	0.000	0.000	0.006	0.191	0.062
	$T(4,\pm 2)$	0.000	0.000	−0.005	−0.151	−0.049
54.7°	$T(0,0)$	13.857	5.134	100.541	4.821	11.962
	$T(2,0)$	0.000	−0.272	−0.007	−0.473	−0.221
	$T(2,\pm 1)$	0.000	∓0.232	∓0.399	∓0.289	∓0.318
	$T(2,\pm 2)$	0.000	0.170	0.272	0.251	0.244
	$T(4,0)$	0	0	0	0	0
	$T(4,\pm 1)$	0.000	0.000	∓0.007	∓0.219	∓0.070
	$T(4,\pm 2)$	0.000	0.000	0.003	−0.110	−0.035

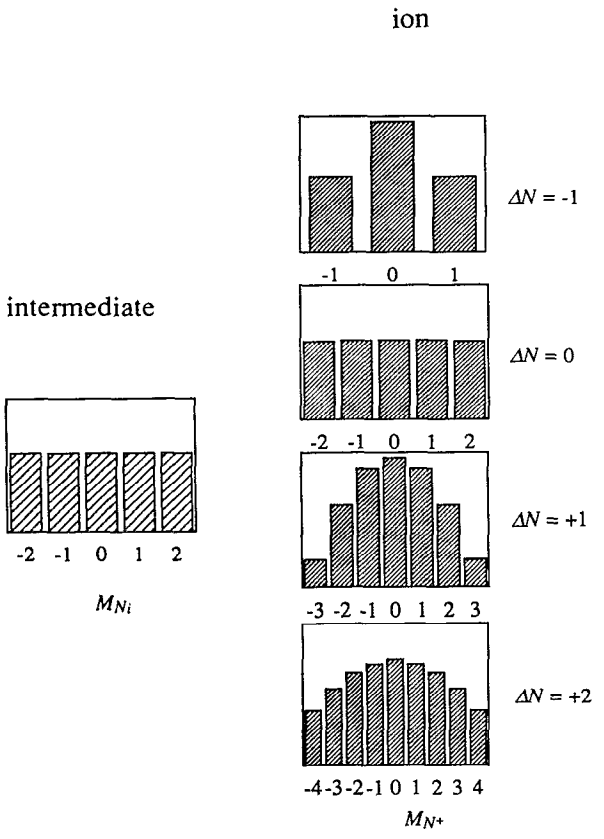

FIG. 9. Relative populations of the Zeeman sublevels ($^N\rho M_N, M_N$) for each ion rotational state following ionization of the level populated by a $Q_1(2.5)$ transition. The excitation–ionization geometry is $\Theta_I = 54.7°$. For comparison, the M_{N_i} populations are also shown. Coherences between sublevels are not represented.

tional level, N^+, of the ion for a given set of dynamical parameters. In Table IV we present the state multipoles that describe the ion alignment following excitation via the $Q_1(2.5)$ transition for our three excitation–ionization geometries. In general, the ion alignment resembles that of the intermediate state; this resemblance is especially strong for $\Delta N=0$. This observation illustrates that, as expected, the much lighter electron carries away most of the dynamical information. Indeed, by measuring the photoelectron angular distribution alone we can predict the ion alignment; the converse does not follow. The $\Delta N=0$ ions show very little change in alignment. This result can be seen clearly in Fig. 9, where we present M_{N^+} populations for each ion rotational state for the magic-angle geometry. Although the intermediate state M_{N_i} sublevels are equally populated, the M_{N^+} sublevels of the $\Delta N\neq 0$ ions are not. A possible rationalization of this in terms of the nonatomic character of the NO $A\,^2\Sigma^+$ state is given in the following paper.[7]

IV. CONCLUSION

We have presented a treatment that includes the coherence terms that result from breaking cylindrical symmetry in a $(1+1')$ REMPI process with two light beams that have independently rotatable linear polarizations. Coherences cause the presence of $T(2,\pm 1)$ and $T(2,\pm 2)$ state multipoles in the intermediate state, and the resulting interference terms give rise to $\beta_{2,M\neq 0}$ and $\beta_{4,M\neq 0}$ terms that contribute to the photoelectron angular distributions. These terms give rise to a complicated θ dependence and a ϕ dependence of the PAD. The observation of a deviation from either cylindrical $[I(\phi)=\text{const}]$ or reflection symmetry $[I(\theta,\phi)=I(-\theta,\phi)]$ in a PAD is a manifestation of coherence.

From rotationally resolved PADs, we can characterize the photoelectron wave function and thus deduce other dynamical observables such as ion alignment. Our formalism makes this particularly facile. The effects of breaking cylindrical symmetry are marked in some cases and cannot be neglected by the experimentalist in extracting dynamical information from observed photoelectron angular distributions.

ACKNOWLEDGMENTS

K. L. R. thanks the SERC for a NATO postdoctoral fellowship. We are grateful to Sarah Allendorf and Jinchun Xie for useful discussions. We acknowledge the support of the U. S. Air Force Office of Scientific Research under contract AFOSR 89 0264 and the National Science Foundation under Grant No. PHY-9020457.

APPENDIX A

The matrix element appropriate for the ionization step can be written[26]

$$\langle N^+\Lambda^+ M_{N^+}|\langle \mathbf{k},l\lambda m_l|1\mu_\lambda 0|N_i\Lambda_i M_{N_i}\rangle, \tag{A1}$$

where

$$|\mathbf{k},l\lambda m_l\rangle = i^l Y^*_{lm_l}(\hat{k}) D^{l*}_{m_l\lambda}(\hat{R}) \tag{A2}$$

and

$$|N\Lambda M_N\rangle = \sqrt{2N+1}\, D^{N*}_{M_N\Lambda}(\hat{R}). \tag{A3}$$

Thus, the integral becomes

$$\int \left[\sqrt{2N^++1}\, D^{N^+*}_{M_{N^+}\Lambda^+}(\hat{R}) i^l Y^*_{lm_l}(\theta,\phi) D^{l*}_{m_l\lambda}(\hat{R})\right]^* \times D^{1*}_{0\mu_\lambda}(\hat{R})\sqrt{2N_i+1}\, D^{N_i*}_{M_{N_i}\Lambda_i}(\hat{R}) r_{l\lambda} e^{i\eta_{l\lambda}} d\hat{R}. \tag{A4}$$

Using the identity[15]

$$D^l_{m\lambda}(\hat{R}) D^{1*}_{0\mu_\lambda}(\hat{R}) = (-1)^{-\mu_\lambda} \sum_{N_t} (-1)^{M_{N_t}-\Lambda_t}(2N_t+1) \times \begin{pmatrix} l & 1 & N_t \\ m_l & 0 & M_{N_t} \end{pmatrix} \begin{pmatrix} l & 1 & N_t \\ \lambda & -\mu_\lambda & \Lambda_t \end{pmatrix} \times D^{N_t}_{-M_{N_t}-\Lambda_t}(\hat{R}), \tag{A5}$$

we obtain after integration

$$\langle N^+\Lambda^+ M_{N^+}|\langle \mathbf{k},l\lambda m_l|1\mu_\lambda 0|N_i\Lambda_i M_{N_i}\rangle = \sqrt{(2N^++1)(2N_i+1)} \sum_{N_t}(2N_t+1)(-1)^{M_{N^+}+\Lambda^++\mu_\lambda}(-i)^l Y_{lm_l}(\theta,\phi) r_{l\lambda} e^{i\eta_{l\lambda}} \times \begin{pmatrix} l & 1 & N_t \\ m_l & 0 & M_{N_t} \end{pmatrix} \begin{pmatrix} l & 1 & N_t \\ \lambda & -\mu_\lambda & \Lambda_t \end{pmatrix} \begin{pmatrix} N^+ & N_t & N_i \\ M_{N^+} & -M_{N_t} & -M_{N_i} \end{pmatrix} \begin{pmatrix} N^+ & N_t & N_i \\ \Lambda^+ & -\Lambda_t & -\Lambda_i \end{pmatrix}. \tag{A6}$$

[1] S. W. Allendorf, D. J. Leahy, D. C. Jacobs, and R. N. Zare, J. Chem. Phys. **91**, 2216 (1989).
[2] K. S. Viswanathan, E. Sekreta, E. R. Davidson, and J. P. Reilly, J. Phys. Chem. **90**, 5078 (1986).
[3] M. A. O'Halloran, P. M. Dehmer, S. T. Pratt, J. L. Dehmer, and F. S. Tomkins, J. Chem. Phys. **90**, 930 (1989).
[4] H. Rudolph and V. McKoy, J. Chem. Phys. **91**, 2235 (1989).
[5] K. L. Reid, D. J. Leahy, S. W. Allendorf, and R. N. Zare, in *Resonance Ionization Spectroscopy 1990* (Institute of Physics, Bristol, 1991). Please note that the $M = \pm 1$ terms have been neglected in this reference. Accordingly, in this reference Fig. 2 is in error.
[6] A. C. Kummel, G. O. Sitz, and R. N. Zare, J. Chem. Phys. **88**, 6707 (1988).
[7] D. J. Leahy, K. L. Reid, and R. N. Zare, J. Chem. Phys. **95**, 1757 (1991).
[8] J. C. Tully, R. S. Berry, and B. J. Dalton, Phys. Rev. **176**, 95 (1968).
[9] G. Leuchs and H. Walther, in *Multiphoton Ionization of Atoms* edited by S. L. Chin and P. Lambropoulos (Academic, Toronto, 1984), p. 109.
[10] S. J. Smith and G. Leuchs, Adv. At. Mol. Phys. **24**, 157 (1988).
[11] S. N. Dixit and V. McKoy, J. Chem. Phys. **82**, 3546 (1985).
[12] S. N. Dixit and P. Lambropoulos, Phys. Rev. A **27**, 861 (1983).
[13] K. Blum, *Density Matrix Theory and Applications* (Plenum, New York, 1981).
[14] R. L. Dubs and V. McKoy, J. Chem. Phys. **91**, 5208 (1989).
[15] R. N. Zare, *Angular Momentum* (Wiley, New York, 1988).
[16] J. Xie and R. N. Zare (in preparation).
[17] J. A. Duncanson, M. P. Strand, A. Lingard, and R. S. Berry, Phys. Rev. Lett. **37**, 987 (1976).
[18] J. C. Hansen, J. A. Duncanson, R. -L. Chien, and R. S. Berry, Phys. Rev. A **21**, 222 (1980); O. C. Mullins, R. -L. Chien, J. E. Hunter, J. S. Keller, and R. S. Berry, *ibid.* **31**, 321 (1985) and references therein.
[19] G. Leuchs, S. J. Smith, S. N. Dixit, and P. Lambropoulos, Phys. Rev. Lett. **56**, 708 (1986).
[20] S. Basile, F. Trombetta, and G. Ferrante, Phys. Rev. Lett. **61**, 2435 (1988).
[21] J. C. Hansen and R. S. Berry, J. Chem. Phys. **80**, 4078 (1984).
[22] R. L. Dubs, S. N. Dixit, and V. McKoy, J. Chem. Phys. **85**, 6267 (1986); V. McKoy, and S. N. Dixit, *ibid* **88**, 968 (1988).
[23] J. R. Appling, M. G. White, T. M. Orlando, and S. L. Anderson, J. Chem. Phys. **85**, 6803 (1986); J. R. Appling, M. G. White, R. L. Dubs, S. N. Dixit, and V. McKoy, *ibid.* **87**, 6927 (1987); C. Westphal, J. Bansmann, M. Getzlaff, and G. Schoenhense, Phys. Rev. Lett. **63**, 151 (1989).
[24] H. Rudolph, V. McKoy, and S. N. Dixit, J. Chem. Phys. **90**, 2570 (1989).
[25] J. Cooper and R. N. Zare, J. Chem. Phys. **48**, 764 (1968).
[26] A. D. Buckingham, B. J. Orr, and J. M. Sichel, Philos. Trans. R. Soc. Lond. Ser. A **268**, 147 (1970).